The Interplay Between the Electro-Magnetic and Wave-Induced Instability Mechanisms in the Hyperloop Transportation System

Fărăgău, Andrei B.; Wang, Rui; Metrikine, Andrei V.; van Dalen, Karel N.

Important note
To cite this publication, please use the final published version (if applicable).
Please check the document version above.

The Interplay Between the Electro-Magnetic and Wave-Induced Instability Mechanisms in the Hyperloop Transportation System

Andrei B. Fărăgău, Rui Wang, Andrei V. Metrikine, and Karel N. van Dalen

1 Introduction

Hyperloop is a new emerging transportation system that is in the development stage. Its design minimises the air resistance by having the vehicle travel inside a depressurised tube (near vacuum) and eliminates the wheel-rail contact friction by using an electro-magnetic suspension, similar to the ones used by Maglev trains. By doing so, it can potentially reach much higher velocities than conventional railways, thus being a climate-friendly competitor to air transportation.

Many challenges faced by the Hyperloop system have already been identified and investigated in the context of high-speed railways. However, due to the much larger target velocities, new challenges will most likely be encountered [8, 13]. One such a challenge is ensuring the dynamic stability of the system at large velocities and avoiding excessive amplifications of the response. It is well known that the vibration of a vehicle travelling on an elastic guideway can become unstable when its velocity exceeds a certain critical velocity [2]. Metrikin [11] showed that the physical cause of instability is that the energy associated to the radiation of anomalous Doppler waves, which feed back energy into the vehicle vibration, is larger than the one associated to normal Doppler waves. Knowing in which velocity regimes the Hyperloop system can be unstable (i.e., determining the critical velocities [3]) is of high practical importance for its design.

This study aims to determine the said unstable velocity regimes and, more specifically, is concerned with the interplay between two instability sources, namely (i) the electro-magnetic suspension and (ii) the wave-induced instability. To this end, the Hyperloop system is modelled as an infinite beam continuously supported by a

A. B. Fărăgău (✉) · R. Wang · A. V. Metrikine · K. N. van Dalen
Department of Engineering Structures, Delft University of Technology, Delft, The Netherlands
e-mail: A.B.Faragau@tudelft.nl

viscoelastic foundation subject to a moving mass (see Fig. 1). The vehicle-guideway interaction occurs through a nonlinear electro-magnetic force governed by the suspension system. The electro-magnetic suspension makes the system inherently unstable, thus requiring a control strategy to ensure stability of the system even at quasi-static velocities. In the current work, a basic proportional and derivative (PD) control strategy with constant gains is used. Since the PD control is able to both insert and extract energy from the system, its influence on the system's stability is currently unknown.

The novelty of this work lies in bridging the gap between the structural-dynamics and control-dynamics aspects of the problem. From the structural-dynamics viewpoint, the influence of the electro-magnetic suspension on the stability of an object moving on an infinite guideway has not been previously investigated. From the control-dynamics perspective, the guideway is usually simplified to either a rigid base [7, 14] or a single-degree-of-freedom [9, 15], thus neglecting the frequency and velocity dependent reaction force of the actual guideway. This study makes the first attempt to combine the two aspects and to investigate the interplay of two fundamentally different instability sources.

2 Model and Solution Method

2.1 Model Formulation

The system consists of an infinite Euler-Bernoulli beam with mass per unit length ρ and bending stiffness EI. The beam is continuously supported by distributed springs (k_d) and dashpots (c_d). The guideway is acted upon by a vehicle of mass M moving with velocity v. The vehicle and the guideway are connected through a nonlinear electro-magnetic force F that, similarly to the electro-magnetic suspension in Maglev trains, only works in attraction [14]. For the chosen solution method, it is convenient to write the governing equations in the reference frame moving with the vehicle, i.e., $\xi = x - v\bar{t}$ and $t = \bar{t}$, where $(x, \bar{t})$ and (ξ, t) are the spatial and temporal coordinates in the stationary and moving reference frames, respectively. Figure 1 depicts the system, while its governing equations read [14]

$$EIw'''' + \rho(\ddot{w} - 2v\dot{w}' + v^2 w'') + c_d(\dot{w} - vw') + k_d w = -F(t)\delta(\xi), \tag{1}$$

$$M\ddot{u} = F(t) - Mg, \tag{2}$$

$$F(t) = C\frac{I^2}{(w_0-u)^2}, \tag{3}$$

$$\dot{I} = \frac{w_0-u}{2C}\left(U - IR + 2C\frac{I}{(w_0-u)^2}(\dot{w}_0 - \dot{u})\right), \tag{4}$$

$$U = K_p(w_0 - u - \Delta^{ss}) + K_d(\dot{w}_0 - \dot{u}) + U^{ss}, \tag{5}$$
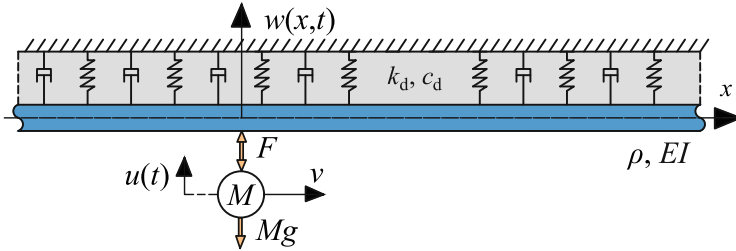
Fig. 1 System schematics: an infinite Euler–Bernoulli beam continuously supported by a viscoelastic foundation subject to a moving mass. The vehicle-structure interaction is governed by the nonlinear electro-magnetic suspension

where primes and overdots denote partial derivatives in space ξ and time t, respectively, g is the gravitational acceleration, δ represents the Dirac delta function, u is the mass displacement, and $w_0 = w(\xi = 0)$ is the beam displacement under the moving mass. The electro-magnetic force F depends on the current intensity I and on the air-gap $\Delta = w_0 - u$, while C is a constant that depends on the electro-magnet properties [14]. Equation (4) is a nonlinear differential equation governing the current intensity where U is the voltage and R is the circuit resistance. Note that F represents just the lift component of the electro-magnetic force while the drag component is neglected. Also, the velocity dependency of the lift component [7] is neglected and could be investigated in future studies.

Without a control strategy, the formulated system is inherently unstable, even when the vehicle is not moving. Consequently, a control strategy on voltage U is imposed (Eq. (5)). A standard proportional and derivative control strategy is used, where K_p and K_d are the position and velocity feedback gains, respectively. The error is defined as the deviation from the desired air-gap Δ^{ss} (superscript ss stands for steady state); U^{ss} represents the voltage that leads to the desired air-gap in the equilibrium state. More complex control strategies can be implemented, but for this investigation, the simple control strategy suffices.

We consider a typical Hyperloop design that was previously described in [6]. Since the current model neglects the discrete nature of the supports, the relevant parameters from [6] are divided by the support spacing to obtain an equivalent distributed foundation. The vehicle is suspended from above and the displacement w is at the rail level (located at the top of the tube). Consequently, the spring stiffness in our phenomenological model accounts not only for the support stiffness but also for the flexibility of the tube-rail connection and, most importantly, for the flexibility introduced by the ovalization of the tube. The parameter values are $EI = 25 \times 10^6$ kNm^2, $\rho = 1400$ kg/m, $k_d = 28 \times 10^3$ kN/m^2, $c_d = 20$ kNs/m^2, $M = 7650$ kg, $C = 0.05$ Nm^2/A^2, and $\Delta^{ss} = 15$ mm.

2.2 Solution Method

Since the system stability is dictated by the vehicle-guideway interaction, it suffices to investigate the response under the moving vehicle (i.e., $\xi = 0$). To this end, the guideway response w_0 under the moving vehicle is written as follows:

$$w_0(t) = -\int_0^t G_0(t - \tau) F(\tau) \mathrm{d}\tau + w_0^{\mathrm{ic}}(t), \qquad (6)$$

where G_0 represents the Green's function of the guideway evaluated at $\xi = 0$ due to a moving impulse load and w_0^{ic} represents free vibrations of the guideway at $\xi = 0$ due to initial conditions corresponding to the system's equilibrium position. This term is necessary because the convolution integral captures just the response of the system with trivial initial conditions. Note that to obtain Eq. (6) from Eq. (1) no assumptions or approximations have been made, with the only restriction that Eq. (6) limits the observation to the position of the vehicle. Also, the partial-differential equation of the beam is not explicit in Eq. (6) but is accounted for through the non-local nature of the Green's function G_0.

This Green's function G_0 can be obtained from Eq. (1) by replacing F with $-\delta(t)$. The ensuing equation can be solved by applying the Laplace transform over time and expressing the Laplace-domain solution as a superposition of wave modes [5]. The resulting analytical solution is evaluated at $\xi = 0$ to obtain $\hat{G}_0$ (the hat represents the quantity in the Laplace domain). Its time-domain counterpart G_0 is obtained by evaluating the inverse Laplace transform numerically.

To solve the system of Eqs. (2)–(6), we first approximate the convolution integral by discretising time and assuming that the electro-magnetic force has a linear variation inside one time step, obtaining the following expression [4]

$$w_{0,n} = \sum_{\bar{n}=0}^{n-1} \left[F_{\bar{n}}(w_{0,\bar{n}}) \mathcal{L}_{n-\bar{n}-1} + F_{\bar{n}+1}(w_{0,\bar{n}+1}) \mathcal{R}_{n-\bar{n}-1} \right] + w_{0,n}^{\mathrm{ic}}, \qquad n \geq 1, \tag{7}$$

$$\mathcal{L}_{n-\bar{n}-1} = \int_{t_{\bar{n}}}^{t_{\bar{n}+1}} G_0(t_n - \tau) \left(1 - \frac{\tau - t_{\bar{n}}}{\Delta t} \right) \mathrm{d}\tau, \tag{8}$$

$$\mathcal{R}_{n-\bar{n}-1} = \int_{t_{\bar{n}}}^{t_{\bar{n}+1}} G_0(t_n - \tau) \frac{\tau - t_{\bar{n}}}{\Delta t} \mathrm{d}\tau, \tag{9}$$

where n is the observation time index while $\bar{n}$ is the running (integration) time index. Equation (7) is valid only for $n \geq 1$ because the response is described by the initial conditions (incorporated in $w_{0,n}^{\mathrm{ic}}$) at $t_0 = 0$. $\mathcal{L}$ and $\mathcal{R}$ represent the responses observed at t_n due to triangular pulses lasting between $t_{\bar{n}}$ and $t_{\bar{n}+1}$.

Equation (7) is implicit for $\bar{n} = n-1$ because the contact force F_n depends on the response $w_{0,n}$. Therefore, the equation is divided into a yet unknown *instantaneous*

contribution and an already known *history* term, leading to

$$w_{0,n} = w_{0,n}^{\text{ic}} + w_{0,n}^{\text{hist}} + F_n(w_{0,n})\mathcal{R}_0, \tag{10}$$

$$w_{0,n}^{\text{hist}} = \sum_{\bar{n}=0}^{n-2}\left[F_{\bar{n}}(w_{0,\bar{n}})\mathcal{L}_{n-\bar{n}-1} + F_{\bar{n}+1}(w_{0,\bar{n}+1})\mathcal{R}_{n-\bar{n}-1}\right] + F_{n-1}(w_{0,n-1})\mathcal{L}_0.$$

Next, F_n (discretised Eq. (3)) is substituted in Eq. (10), resulting in the third-order polynomial

$$w_{0,n}^3 + a_{2,n}w_{0,n}^2 + a_{1,n}w_{0,n} + a_{0,n} = 0, \tag{11}$$

$$a_{2,n} = -w_{0,n}^{\text{ic}} - w_{0,n}^{\text{hist}}, \quad a_{1,n} = -u_n^2, \quad a_{0,n} = \left(w_{0,n}^{\text{ic}} - w_{0,n}^{\text{hist}}\right)u_n^2 + CI_n^2\mathcal{R}_0.$$

The roots of this polynomial can be computed using a symbolic mathematical software (e.g., Maple) and are not given here for brevity. From the three existing roots, only one is physically admissible (i.e., real valued and corresponding to the vehicle below the guideway). The discretised system of equations now reads

$$w_{0,n} = f\left(w_{0,n}^{\text{ic}}, w_{0,n}^{\text{hist}}, u_n, I_n\right), \tag{12}$$

$$M\ddot{u}_n = C\frac{I_n^2}{\left(w_{0,n}-u_n\right)^2} - Mg, \tag{13}$$

$$\dot{I}_n = \frac{w_{0,n}-u_n}{2C}\left(U_n - I_nR + 2C\frac{I_n}{\left(w_{0,n}-u_n\right)^2}(\dot{w}_{0,n} - \dot{u}_n)\right), \tag{14}$$

$$U_n = K_{\text{p}}\left(w_{0,n} - u_n - \Delta^{\text{ss}}\right) + K_{\text{d}}\left(\dot{w}_{0,n} - \dot{u}_n\right) + U^{\text{ss}}, \tag{15}$$

where f represents the expression of the real-valued root of Eq. (11). The resulting system of ordinary differential equations is solved through a time-stepping scheme (i.e., Runge–Kutta in-built in the ODE45 solver in Matlab).

3   Linearisation of the Nonlinear Model

To investigate the system stability, next to the numerical solution it is instructive to study the linearised system around the equilibrium state. Although the system of Eqs. (2)–(6) could have multiple equilibrium positions, we are interested only in the behaviour around the operational equilibrium position (i.e., the standard steady state of an equivalent mechanical system). To this end, a perturbation around the steady state is introduced by substituting $w_0(t) = w_0^{\text{ss}} + w_0^{\text{tr}}(t)$, $u(t) = u^{\text{ss}} + u^{\text{tr}}(t)$, $F(t) = F^{\text{ss}} + F^{\text{tr}}(t)$, $I(t) = I^{\text{ss}} + I^{\text{tr}}(t)$, where superscript tr stands for transient. After mathematical manipulations, we apply the Taylor expansion to the governing

equations corresponding to Eqs. (3) and (4). Thus, the linearised system is obtained and reads

$$w_0^{\text{tr}} = -\int_0^t G_0(t - \tau) F^{\text{tr}}(\tau) \mathrm{d}\tau, \tag{16}$$

$$M\ddot{u}^{\text{tr}} = F^{\text{tr}}, \tag{17}$$

$$F^{\text{tr}} = \frac{2CI^{\text{ss}2}}{\Delta^{\text{ss}3}} \left(\frac{\Delta^{\text{ss}}}{I^{\text{ss}}} I^{\text{tr}} + u^{\text{tr}} - w_0^{\text{tr}} \right), \tag{18}$$

$$\dot{I}^{\text{tr}} = \frac{\Delta^{\text{ss}}}{2C} \left[-I^{\text{tr}} R + K_{\text{p}} \left(w_0^{\text{tr}} - u^{\text{tr}} \right) + \left(K_{\text{d}} + \frac{2CI^{\text{ss}}}{\Delta^{\text{ss}2}} \right) \left(\dot{w}_0^{\text{tr}} - \dot{u}^{\text{tr}} \right) \right]. \tag{19}$$

The stability of the equilibrium state can be investigated through the eigenvalues of the linearised system. To obtain the characteristic equation, the Laplace transform is applied to Eqs. (16)–(19) with respect to time. The expression of the electromagnetic force is substituted in the Laplace-domain counterparts of Eqs. (16) and (17), and the resulting system of equations, in matrix form, reads

$$\begin{pmatrix} 1 - \hat{G}_0(s)\frac{2CI^{\text{ss}2}}{\Delta^{\text{ss}3}} & \hat{G}_0(s)\frac{2CI^{\text{ss}2}}{\Delta^{\text{ss}3}} & \hat{G}_0(s)\frac{2CI^{\text{ss}}}{\Delta^{\text{ss}2}} \\ \frac{2CI^{\text{ss}2}}{\Delta^{\text{ss}3}Ms^2} & 1 - \frac{2CI^{\text{ss}2}}{\Delta^{\text{ss}3}Ms^2} & -\frac{2CI^{\text{ss}}}{\Delta^{\text{ss}2}Ms^2} \\ \frac{(\Delta^{\text{ss}2}K_{\text{d}}+2CI^{\text{ss}})s+\Delta^{\text{ss}2}K_{\text{p}}}{-2C\Delta^{\text{ss}}} & \frac{(\Delta^{\text{ss}2}K_{\text{d}}+2CI^{\text{ss}})s+\Delta^{\text{ss}2}K_{\text{p}}}{2C\Delta^{\text{ss}}} & \frac{\Delta^{\text{ss}}R}{2C} + s \end{pmatrix} \begin{pmatrix} \hat{w}^{\text{tr}} \\ \hat{u}^{\text{tr}} \\ \hat{I}^{\text{tr}} \end{pmatrix} = \begin{pmatrix} 0 \\ f_0 \\ I_0 \end{pmatrix}, \tag{20}$$

where $f_0 = su_0 + v_0$, with u_0, v_0, and I_0 are the initial conditions of the perturbation for the mass and current. The beam is considered unperturbed with respect to the steady state, but perturbations can be imposed through w^{ic}. The characteristic equation, which is not presented here for brevity, is obtained by equating the determinant of the coefficient matrix to zero. It must be emphasised that the characteristic equation is neither a polynomial (since s appears also in $\hat{G}_0$ under square roots) nor a transcendental equation, meaning that it has a finite amount of roots. The eigenvalues are determined numerically by using a root finding routine (i.e., *fsolve* in Matlab) with a multitude of initial guesses for s to cover the part of the complex plane relevant for this problem.

4 Results and Discussion

Figure 2 presents the eigenvalues of the linearised system for set values of control gains K_{p} and K_{d} and for varying vehicle velocity. Note that in this paper, the critical velocity c_{cr} refers to the minimum phase velocity of the guideway (i.e., the velocity at which the load becomes super-critical) and not to the velocity at which stability is lost. It can be seen that the choice of control gains ensures that the system is stable when the vehicle is not moving. Three eigenvalues are found, one real valued
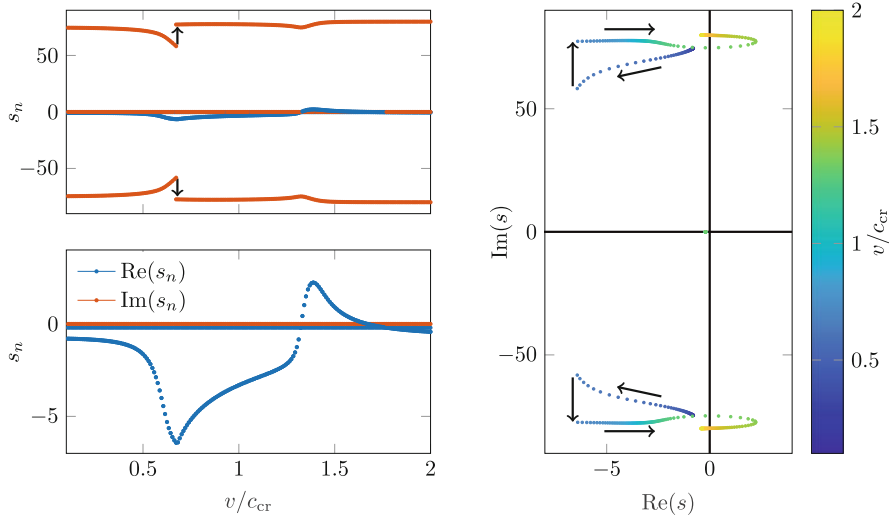
Fig. 2 The eigenvalues versus relative velocity of the vehicle. The bottom left panel is a zoom in of the top left panel. $K_p = 20$ (kV/m), $K_d = 40$ (kVs/m)

and two complex-conjugates, unlike the studies that approximate the guideway by a single-degree-of-freedom system in which five eigenvalues are always found [9, 15]. It must be mentioned that in the range of $v \approx 0.7$–$1.3c_{cr}$ an additional pair of complex-valued roots is found (not presented in Fig. 2) that corresponds to branch points of the characteristic equation introduced by the dynamic stiffness of the infinite guideway. The behaviour of infinite systems (guideway) coupled to finite/discrete ones (vehicle) cannot be fully described by the eigenvalues because the integrals along the branch cuts also influence the dynamic behaviour. However, neither the branch points nor the integrals along the branch cuts influence the system stability and are, therefore, ignored in this analysis. The jump observed in the location of the complex-valued eigenvalues at $v \approx 0.7c_{cr}$ is caused by the eigenvalues crossing the branch cut.

Focusing on the three eigenvalues presented in Fig. 2, the real-valued one remains almost unchanged with varying velocity (most clear in the bottom left and right panels), while the complex-valued ones undergo significant changes with varying velocity. As the velocity approaches c_{cr}, the magnitude of the negative real part of the complex-valued pair increases meaning that the perturbation-induced vibration decays faster if the vehicle velocity is close to the critical one. This suggests that the increase in velocity (for sub-critical velocities) is beneficial when it comes to suppressing perturbations. At a velocity of approximately $1.3c_{cr}$, the real part of the complex-valued eigenvalues becomes positive, meaning that the equilibrium position loses stability through a super-critical Hopf bifurcation. Interestingly, increasing the velocity even further, the equilibrium position regains stability. This feature is not unique to the controlled electro-magnetic suspension since it also
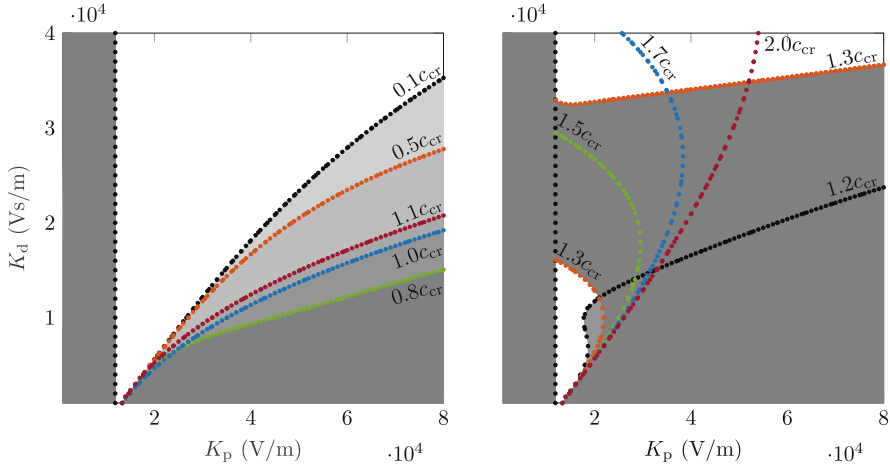
Fig. 3 Stability vs control gains for different vehicle velocities, namely $v = 0.1\text{–}1.1c_{cr}$ (left panel) and $v = 1.2\text{–}2c_{cr}$ (right panel); grey indicates instability. Note that for $v = 1.5\text{–}2c_{cr}$, the instability region is outside the closed ovals and does not have a grey background to avoid cluttering the figure

appears in equivalent mechanical systems [12] with compliant contact relations between the vehicle and guideway.

To offer a general overview, Fig. 3 presents the stability parameter space of the control gains for different vehicle velocities. For all velocities and K_d values, the equilibrium position is unstable if K_p is smaller than a specific minimum $K_{p,min}$ (vertical line in Fig. 3). In such a scenario, the control is not fast enough to counteract the vehicle falling under gravity, thus giving rise to instability. For $K_p > K_{p,min}$, the equilibrium position can be stable. The stability domain monotonically increases with increasing velocity, meaning that the larger K_p the larger should K_d be to ensure stability, reaching its maximum at $v \approx 0.8c_{cr}$, after which it slightly reduces until $v \approx 1.1c_{cr}$. The instability in these scenarios (left panel of Fig. 3) is solely caused by the electro-magnetic levitation system.

The stability parameter space changes drastically from the above description starting at $v \approx 1.2c_{cr}$ (right panel of Fig. 3) and reaches the minimum at $v \approx 1.3c_{cr}$. While at lower velocities the stability domains slightly expand or contract without any qualitative change, at $v \approx 1.3c_{cr}$ and above, the stability domain transits to a closed oval at larger velocities with an additional stable region above a specific K_d value (see almost horizontal line in the right panel). Increasing the velocity even further, the stable parameter space increases in size once again through the expansion of the oval shape. The change in behaviour between the left and right panels in Fig. 3 does not originate from the control system but is caused by the second instability mechanism becoming present. More specifically, the energy radiated by the vehicle into the guideway is being fed back to the vehicle vibration through the anomalous Doppler waves [11]. It is important to emphasise that,
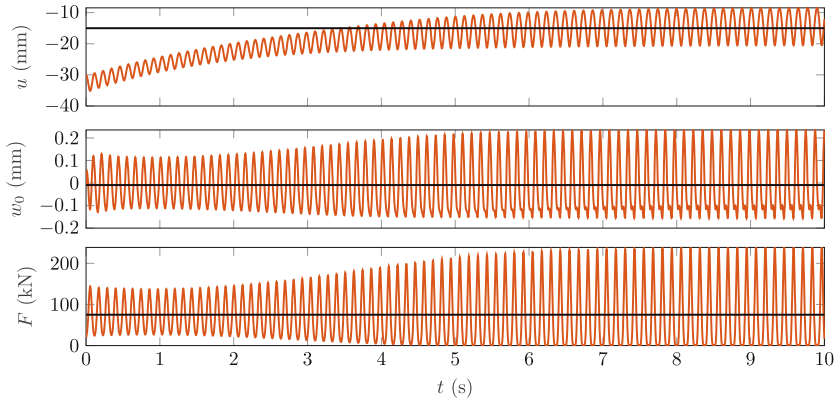
Fig. 4 The time-history response of the nonlinear system; $v = 1.3c_{cr}$, $K_p = 20$ (kV/m), and $K_d = 20$ (kVs/m)

similarly to its mechanical counterpart, this type of instability seems to occur only at super-critical velocities, meaning that the electro-magnetic interaction does not lead to qualitative differences. Furthermore, this instability source cannot be observed when one reduces the guideway to a single-degree-of-freedom system as done in previous studies on maglev trains and, as can be seen, can reduce the stability parameter range drastically.

In the vicinity of the stability boundaries shown in Fig. 3, limit cycles can be observed provided that $K_p > K_{p,min}$. A typical limit cycle is shown in Fig. 4 for a velocity of $v = 1.3c_{cr}$. As can be seen, the electro-magnetic force first increases after which it drops to zero in the limit cycle oscillation, implying that the vehicle is first pulled towards the guideway and the control then reacts by reducing the electro-magnetic force to zero, basically leading to a free falling body; after this, the electro-magnetic force increases again to avoid the vehicle dropping under gravity. If K_p is far away from the stability boundary, the control becomes very aggressive and overshoots, leading to the vehicle colliding with the guideway, moment at which the electro-magnetic force becomes infinite. Thus, for very large values of K_p, limit cycles no longer exist. Limit cycles are also observed in equivalent mechanical systems provided that either the contact force [10] or the guideway [1] has a nonlinear behaviour. Nonetheless, limit cycles in mechanical systems are only observed at super-critical velocities because the radiated energy feedback is the sole instability mechanism, while the Hyperloop system exhibits limit cycles at any velocity due to the electro-magnetic induced instability.

5   Conclusions

From a practical viewpoint, this study investigated the unstable velocity regimes of the Hyperloop vehicle-structure interaction and their dependency on the control gains. From a theoretical perspective, this paper studied the interplay of two fundamentally different instability mechanisms that are present in the Hyperloop system, namely (i) the electro-magnetic suspension and (ii) the wave-induced instability. To enable the studying of the aforementioned interplay, the velocity and frequency dependent reaction force of the infinite guideway is incorporated in the stability analysis, thus allowing for the vehicle velocity to influence the instability. This is not possible in approaches found in literature where the guideway is either considered rigid or is approximated by a single-degree-of-freedom system. The novelty of this work lies mainly in its theoretical perspective.

It was shown that, for sub-critical velocities, the frequency and velocity dependent reaction force provided by the guideway can be beneficial in suppressing perturbations and in increasing the parameter space in which the system is stable. However, at some super-critical velocities, the stable parameter space reduces drastically. This drastic change is caused by the second instability mechanism, i.e., the radiated energy feedback associated to the anomalous Doppler waves excited at super-critical velocities. Furthermore, in the vicinity of the stability boundaries, the system presents limit cycle oscillations (i.e., stability loss occurs through a super-critical Hopf bifurcation), but for even larger control gains, the limit cycles no longer exist. To conclude, it was shown that the interplay between the two instability mechanisms does not lead to significant qualitative changes compared to considering each mechanism separately.

References

1. Chen, J., Chen, S., Hsu, W.: Effects of geometric nonlinearity on the response of a long beam on viscoelastic foundation to a moving mass. J. Sound Vibr. **497**, 115961 (2021)
2. Denisov, G., Kugusheva, E., Novikov, V.: On the problem of the stability of one-dimensional unbounded elastic systems. J. Applied Math. Mech. **49**(4), 533–537 (1985)
3. Dimitrovová, Z.: On the critical velocity of moving force and instability of moving mass in layered railway track models by semi-analytical approaches. Vibration **6**(1), 113–146 (2023)
4. Fărăgău, A.B., Keijdener, C., de Oliveira Barbosa, J.M., Metrikine, A.V., van Dalen, K.N.: Transition radiation in a nonlinear and infinite one-dimensional structure: a comparison of solution methods. Nonlinear Dyn. **103**, 1365–1391 (2021)
5. Fărăgău, A.B., Mazilu, T., Metrikine, A.V., Lu, T., van Dalen, K.N.: Transition radiation in an infinite one-dimensional structure interacting with a moving oscillator—the Green's function method. J. Sound Vibr. **492**, 115804 (2021)
6. Fărăgău, A.B., Metrikine, A.V., van Dalen, K.N.: Dynamic Amplification in a Periodic Structure Subject to a Moving Load Passing a Transition Zone: Hyperloop Case Study. In: Recent Trends in Wave Mechanics and Vibrations, vol. 125 (2023)

7. Galluzzi, R., Circosta, S., Amati, N., Tonoli, A., Bonfitto, A., Lembke, T.A., Kertész, M.: A multi-domain approach to the stabilization of electrodynamic levitation systems. J. Vibr. Acoustics **142**(6), 061004 (2020)
8. Gkoumas, K.: Hyperloop academic research: a systematic review and a taxonomy of issues. Appl. Sci. **11**(13), 5951 (2021)
9. Hu, J., Ma, W., Chen, X., Luo, S.: Levitation stability and Hopf bifurcation of EMS maglev trains. Math. Probl. Eng. **2020**, 1–20 (2020)
10. Mazilu, T.: Instability of a train of oscillators moving along a beam on a viscoelastic foundation. J. Sound Vib. **332**(19), 4597–4619 (2013)
11. Metrikin A.V.: Unstable vertical oscillations of an object moving uniformly along an elastic guide as a result of an anomalous Doppler effect. Acoust. Phys. **40**(1), 85–89 (1994)
12. Metrikine, A., Popp, K.: Instability of vibrations of an oscillator moving along a beam on an elastic half-space. European J. Mech. A/Solids **18**(2), 331–349 (1999)
13. Museros, P., Lázaro, C., Pinazo, B., Monleón, S.: Key aspects in the analysis and design of Hyperloop™infrastructure under static, dynamic and thermal loads. Eng. Struct. **239**, 112177 (2021)
14. Wu, H., Zeng, X., Gao, D., Lai, J.: Dynamic stability of an electromagnetic suspension maglev vehicle under steady aerodynamic load. Appl. Math. Model. **97**, 483–500 (2021)
15. Xu, J., Chen, C., Gao, D., Luo, S., Qian, Q.: Nonlinear dynamic analysis on maglev train system with flexible guideway and double time-delay feedback control. J. Vibroeng. **19**(8), 6346–6362 (2017)